Print ISSN : 0022-2755
Journal of Mines, Metals and Fuels
Contents available at: www.informaticsjournals.com/index.php/jmmf

Effect of Wall-Slip and Non-Newtonian Fluid on the Steady-State Performance of a Three-Lobe Bearing

Amar Murthy Ambekar and Raghunandana K*

[1,2]*Department of Mechanical and Industrial Engineering, Manipal Institute of Technology, Manipal Academy of Higher Education, Manipal, Karnataka, India.* **Email: raghu.bhat@manipal.edu*

Abstract

The current work investigates the effect of wall-slip on the steady-state performance characteristics of three-lobe journal bearing operating with non-Newtonian lubricant. The power-law model is used to incorporate the non-Newtonian lubricant, while the Navier-slip boundary criteria is used to apply the wall-slip effect on sliding surfaces. Numerical simulations are performed employing the technique of finite difference to determine the performance characteristics under conditions of steady state. According to the findings of this study, it is revealed that the load-carrying capacity is increased by about 15.38% with a slip-length of B_{lx}= 0.2 when slip occurs on the wall of the journal surface.

Keywords: *Three-lobe, non-Newtonian, wall-slip, Navier-slip, power-law.*

1.0 Introduction

Bearings are the essential components of every rotating machine. Today's high-speed machinery necessitates bearings with exceptional qualities not seen before in plain cylindrical journal bearings. In contrast to standard circular journal bearings, multilobe journal bearings are rising in popularity and playing an increasingly significant role in high-speed machinery. Multi-lobe bearings are gaining popularity because they have a better load-bearing capacity, good stability at higher speeds, optimal temperature owing to enhanced lubricant flow, and lower power loss. Lubricants used in these bearings should have a wide range of qualities along with their inherent capabilities to endure harsh operating conditions. These lubricants become non-Newtonian and operate non-linearly due to the enhancement of lubricant attributes gained by adding additives. This has brought up the primary challenge for most researchers. Mirrored finish surfaces are now achievable because of developments in manufacturing technology. Manufacturers have employed this technique on sliding surfaces to reduce friction, resulting in one of the reasons for wall slip between the solid-lubricant contact. Many researchers have discovered experimentally that the previously accepted 'no-slip' boundary condition is no longer applicable for most designed surfaces as there exists a wall slip at the liquid-solid interface when fluid flows against the non-wettable surface. Thus wall-slip is an additional aspect in addition to the formerly mentioned non-Newtonian case. Hence, a conventional Reynolds equation may not be suitable to address these challenges. There is a need to develop a precise mathematical model to overcome these challenges.

**Corresponding Author*

2.0 Literature Review

To address the first concern raised in the preceding section, the use of non-Newtonian fluids, several researchers revealed an awareness in examining the impact of non-Newtonian fluids on bearing performance. It was discovered that in comparison with Newtonian fluids, the couple-stress parameter of a non-Newtonian fluid creates a substantial

impact on the multi-lobe bearing performance characteristics (Crosby & Chetti, 2009). Study of lobed bearings lubricated by micropolar lubricant demonstrated that the micropolar lubricant may improve the static performance characteristics significantly (Khonsari & Brewe, 2008; Rahmatabadi et al., 2010). At all eccentricity ratios, load, side leakage, and friction were found to be lower for pseudoplastic lubricants and greater for dilatant lubricants as matched to Newtonian fluids (Tayal et al., 1982). Not only in laminar conditions but even in the turbulence regime, non-Newtonian fluid showed superior performance characteristics (Soni & DP, 2015). Compared to an equivalent purely viscous fluid, Dilatant lubricants enhance the load-carrying capacity, whereas pseudoplastic lubricants diminish load-carrying capacity (Nessil et al., 2013). With micropolar fluids, the bearing demonstrated a noteworthy improvement in load carrying capacity and a decrease in friction when operated at a lower width to diameter ratio and a high eccentricity ratio (Tsai-Wang Huang et al., 1988). Aside above-listed characteristics, the prevalence of wall-slip on a particular surface influences the bearing's performance (A & K, 2022). Non-circular bearings with non-Newtonian lubricant, mainly when slip occurs on the surface of the journal, substantially impact bearing performance compared to the effect created by wall-slip occurring on the bearing surface. When matched to the typical non-slip situation, the tribological performances of bearings with wall-slip are different and more significant (Bhushan et al., 2009; Rothstein, 2009). Reduction in friction and increased load-bearing capability is achieved with wall slip on the bearing surfaces (Fortier & Salant, 2005; H. A. Spikes, 2003; H. Spikes & Granick, 2003). The position and extent of the slip surface can take a major impact on the load-carrying capability of journal bearings (Lin et al., 2015). Journal bearings with an acceptable slipping surface had an inferior friction coefficient and a greater bearing capacity (Wu, 2008). Bearings having no-slip/slip areas exhibited similar tribological performance to bearings with partially textured surfaces (Aurelian et al., 2011). The three-lobe bearing was determined to have the extreme load-carrying capacity and the lowest friction variable out of four diverse bearing configurations evaluated using non-Newtonian lubricants specified by the power-law model (Das & Roy, 2018). A non-Newtonian lubricant, also known as a couple stress fluid, which is a fluid mixed with polymer additives, enhanced the static characteristics of bearings with three lobes when matched to bearings oiled with Newtonian fluids (Chetti & Crosby, 2019). In either Newtonian or non-Newtonian lubricated slider or multilobe bearings, partial slip-textures have demonstrated favourable impacts, higher load support, and stability possibilities with decreased friction. (Rao, 2010; Rao et al., 2019).

Thus, it is found that researchers have mostly concentrated on the solitary influence of either the 'non-Newtonian influence' or the 'slip effect' and to some extent to the combined effect but only on slider bearings or simple journal bearings. This reveals the fact that no research is carried out on the combined effect of wall-slip and non-Newtonian on three-lobe journal bearings. Therefore, the objective of the present work is to ascertain how wall-slip affects the steady-state performance of a bearing with three lobes by means of a non-Newtonian lubricant. The non-Newtonian effect is incorporated using the power-law model, and the wall-slip effect is applied to sliding surfaces using the Navier-slip boundary criterion. The performance characteristics assessed using numerical simulations and a finite difference approach includes pressure, load-carrying capacity, flow rate, and friction under steady-state settings.

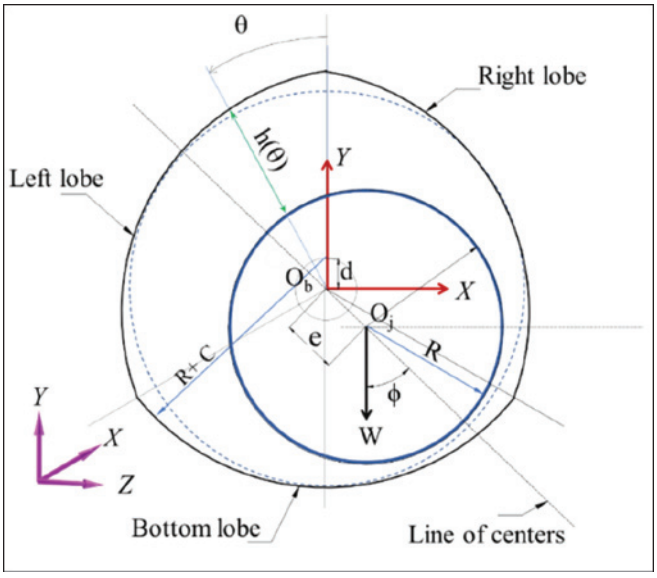


Figure 1: Co-ordinates system and geometry of journal bearing with three lobes

3.0 Analysis

3.1 Three-lobe Bearing Configuration

A three-lobe journal bearing is made up of three bores with their centers offset from the actual shaft center in the vertical direction, reducing clearance in that direction. Fig.1 depicts the three-lobe journal bearing geometry with the employed coordinate system. At the bearing center, each lobe subtends an angle of 120°. The trigonometry relations (Pinkus & Sternlicht, 1961) for the individual lobe and eccentricity ratio are given from Eq.1 to Eq.6.

For bottom lobe,

$$\varepsilon_B=\sqrt{\varepsilon^2+\delta^2+2\varepsilon\delta\cos\phi} \quad \text{... (1)}$$

$$\phi_B = \sin^{-1}\left(\frac{\varepsilon \sin\phi}{\varepsilon_B}\right) \quad \text{... (2)}$$

For right side lobe,

$$\varepsilon_R = \sqrt{\varepsilon^2+\delta^2-2\varepsilon\delta\cos\left(\frac{\pi}{3}+\phi\right)} \quad \text{... (3)}$$

$$\phi_R = \frac{2\pi}{3} - \sin^{-1}\left(\frac{\varepsilon \sin\left(\frac{\pi}{3}+\phi\right)}{\varepsilon_R}\right) \quad \text{... (4)}$$

For left side lobe,

$$\varepsilon_L = \sqrt{\varepsilon^2+\delta^2-2\varepsilon\delta\cos\left(\frac{\pi}{3}-\phi\right)} \quad \text{... (5)}$$

$$\phi_L = \sin^{-1}\left(\frac{\varepsilon \sin\left(\frac{\pi}{3}-\phi\right)}{\varepsilon_L}\right) \quad \text{... (6)}$$

3.2 Modified Reynolds Equation

Earlier, a modified Reynolds equation was established (Chen et al., 2013) to study the impact of boundary slippage on simple journal bearings using the Navier slip boundary condition. In the current study, an extended altered Reynolds equation is developed grounded on the established model and is given in Eq.7. This extended Reynolds equation is novel in that it has the potential to account for the impact of lubricant with non-Newtonian behaviour in conjunction with wall slippage in a three-lobe journal bearing

$$\frac{\partial}{\partial x}\left[\psi(h,n,b_{ix})\frac{\partial p}{\partial x}\right] + \frac{\partial}{\partial z}\left[\psi(h,n,b_{iz})\frac{\partial p}{\partial z}\right] = \frac{1}{2}\frac{\partial h}{\partial x}U_x \quad \text{...(7)}$$

Where,

$$\psi(h,n,b_{ix}) = \frac{h^3}{12\mu' n}\left[\frac{3}{h}\frac{\Delta x_n}{\Delta x_d} - 2\right];\ \psi(h,n,b_{iz})$$

$$= \frac{h^3}{12\mu'}\left[\frac{3}{h}\frac{\Delta z_n}{\Delta z_d} - 2\right];\ \mu' = m\left(\frac{u_b}{h}\right)^{n-1}$$

$$U_x = \left[2u_{1x} + \frac{V_x(h+2b_{1x})}{\Delta x_d}\right];$$

$$\Delta x_n = h^2 + 2h(b_{1x}+b_{2x}) + 4b_{1x}b_{2x};$$

$$\Delta z_n = h^2 + 2h(b_{1z}+b_{2z}) + 4b_{1z}b_{2z};$$

$$\Delta x_d = h + b_{1x} + b_{2x};\ \Delta z_d = h + b_{1z} + b_{2z}$$

At a particular circumferential angle (θ), the dimensionless film thickness can be determined using $\bar{h} = 1 + \bar{\varepsilon}_k cos(\theta - \phi_k)$,

where k represents the left, right or bottom lobe and $\varepsilon = \bar{\varepsilon}_k\ (1-\delta)$. The non-dimensionlised form of Eq. (7) by using the following substitutions is presented in Eq.(8).

$\theta = \frac{x}{R}$, $\bar{z} = \frac{2z}{L}$, $\bar{P} = \frac{pC^{n+1}}{m\omega^n R^{n+1}}$, The dimensionless slip-lengths are $B_{ix} = \frac{b_{ix}}{C}$, $B_{iz} = \frac{b_{iz}}{C}$ $(i = 1,2)$

$$\frac{\partial}{\partial\theta}\left[\psi(\bar{h},n,B_{ix})\frac{\partial\bar{P}}{\partial\theta}\right] + \frac{\partial}{\partial\bar{z}}\left(\frac{D}{L}\right)^2\left[\psi(\bar{h},n,B_{iz})\frac{\partial\bar{P}}{\partial\bar{z}}\right] \quad \text{... (8)}$$

Where,

$$\psi(\bar{h},n,B_{ix}) = \frac{\bar{h}^{-n+2}}{n}\left[\frac{3}{\bar{h}}\frac{\Delta X_n}{\Delta X_d} - 2\right];$$

$$\psi(\bar{h},n,B_{iz}) = \frac{\bar{h}^{2+n}}{n}\left[\frac{3}{\bar{h}}\frac{\Delta Z_n}{\Delta Z_d} - 2\right];$$

$$\Delta X_d = \bar{h} + B_{1x} + B_{2x};\ \Delta Z_d = \bar{h} + B_{1z} + B_{2z};$$

$$\Delta X_n = \bar{h}^2 + 2\bar{h}(B_{1x}+B_{2x}) + 4B_{1x}B_{2x};$$

$$\Delta Z_n = \bar{h}^2 + 2\bar{h}(B_{1z}+B_{2z}) + 4B_{1z}B_{2z};$$

$$H = \frac{\bar{h}(\bar{h}+2B_{2x})}{\Delta X_d}$$

The above Eq. 8 reduces to the standard Reynolds equation as given by Eq.9 by setting the power-law index to unity (n=1, indicating Newtonian fluid) and the slip lengths (B_{1z}, B_{2z}, B_{1x}, and B_{2x}) to zero.

$$\frac{\partial}{\partial\theta}\left(\bar{h}^3\frac{\partial\bar{P}}{\partial\theta}\right) + \left(\frac{D}{L}\right)^2\frac{\partial}{\partial\bar{z}}\left(\bar{h}^3\frac{\partial\bar{P}}{\partial\bar{z}}\right) = 6\frac{\partial\bar{h}}{\partial\theta} \quad \text{... (9)}$$

3.3 Boundary Conditions

The adopted conditions at the boundary are based on the Reynolds boundary condition and are as mentioned below:

$\bar{P}=0$ at extreme edges along Z, i.e, at $\bar{z}=0$ and $\bar{z}=1$

$\bar{P}=0$ at $\theta = 0$ and $\theta = 2\pi$

$$\bar{P} = \left(\frac{\partial\bar{P}}{\partial\theta}\right)_{\theta_s<\theta<\theta_c} = 0$$

Where θ_s and θ_c are start and cavitate point of fluid film.

3.4 Methodology

The computation of pressure developed in the lubricant film domain is approved by discretizing the unwrapped lubricant film domain using the method of finite difference. The mesh view thus obtained by unwrapping is shown in Fig.2.

By nourishing the boundary necessities, a Gauss Seidel repetition tactic is adopted to converge the pressure using successive over relaxation method. The repetition process continues until a pressure convergence of less than 10^{-4} is attained.

Further, the steady-state pressures which are converged is utilized to estimate the related attitude angle by assessing force components along and across the line of centres. The attitude angle is gradually altered until it reaches its final value. Once the pressure and attitude angle fulfil the convergence requirements, the steady-state performance characteristics are computed. The flow chart in Fig.3 depicts

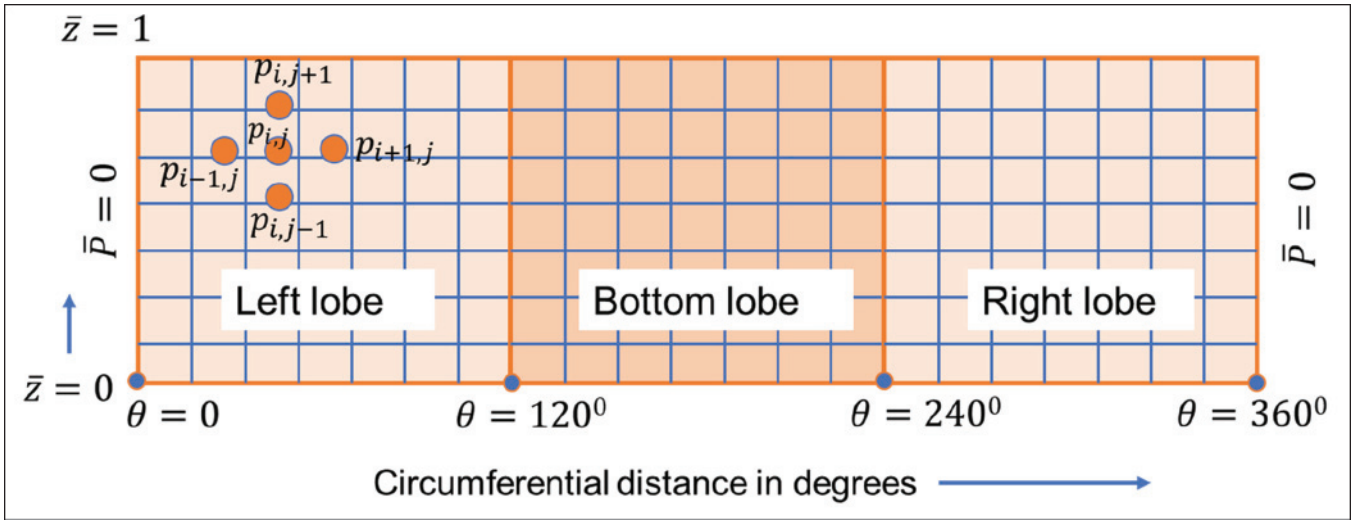


Figure 2: Finite difference mesh representing the three lobes

the whole procedure used in this investigation to determine steady-state parameters.

3.5 Steady State Performance Characteristics

(a) Load Capacity and Sommerfeld Number

Dimensionless pressure developed in the bearing lobes are integrated around the area to determine the effective load carrying capacity. The net load is calculated using two dimensionless load components. The first component ($\bar{W}_\varepsilon$), acts along the line of centres of bearing and journal, and the second component ($\bar{W}_\phi$) acts perpendicular to the line of centers. Eq.10 and Eq.11 represents these dimensionless load components. Once these dimensionless components are obtained, the entire load that the three-lobe journal bearing can support is obtained using the consequential of the above two components and is represented in Eq.12

$$\bar{W}_\varepsilon = -\int_0^1 \int_{\theta_s}^{\theta_c} \bar{P} \cos\theta \, \partial\theta \, \partial\bar{z} \quad \ldots (10)$$

$$\bar{W}_\phi = \int_0^1 \int_{\theta_s}^{\theta_c} \bar{P} \sin\theta \, \partial\theta \, \partial\bar{z} \quad \ldots (11)$$

$$\bar{W} = \sqrt{\bar{W}_\varepsilon^2 + \bar{W}_\phi^2} \quad \ldots (12)$$

The load, $\bar{W}$, thus obtained in Eq. 12 can be used to compute the Sommerfeld number using Eq.13

$$S = \frac{1}{\pi \bar{W}} \quad \ldots (13)$$

(b) Attitude Angle

The load acting on the journal forces it to move away from the line of centers instead of deflecting it co-directionally. The angle formed between the line of centers of the journal and the bearing is called the attitude angle, ϕ. The attituded angle given in Eq.14 is determined readily using the ratio of the load components, $\bar{W}_\varepsilon$ and $\bar{W}_\phi$.

$$\phi = \tan^{-1} \frac{\bar{W}_\phi}{\bar{W}_\varepsilon} \quad \ldots (14)$$

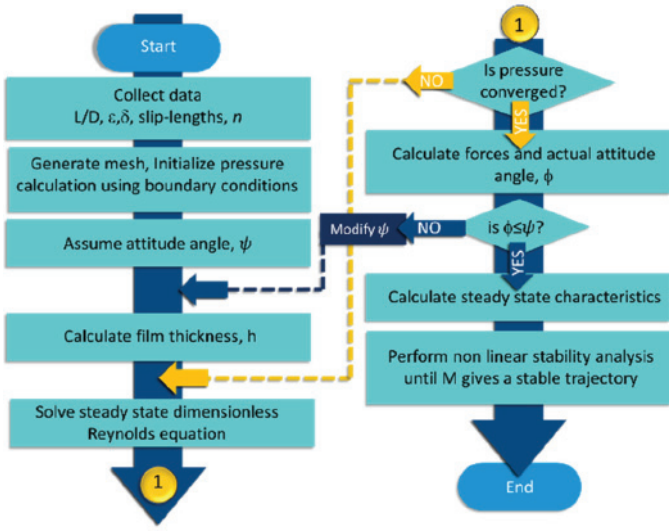


Figure 3: Flowchart representing methodology implemented

(c) Side Leakage

The leakage of oil from the edges of the three lobe bearings is caused due to the gradients of axial pressure. As a result, the oil should be continuously supplied to avoid its depletion in the bearings. The dimensionless end leakage is given in Eq.15

$$\bar{Q}=-\int_{\theta_s}^{\theta_c}\frac{\bar{h}^3}{6}\frac{\partial\bar{P}}{\partial\bar{z}}\Big|_{\bar{z}=1}d\theta \quad \text{... (15)}$$

(c) Friction Force

The friction force is got by integrating the shear stress around the bearing area. Eq.16 represents the dimensionless form of the friction force.

$$\bar{F}=\int_0^1\int_{\theta_s}^{\theta_c}\frac{\bar{h}^3}{2}\left(\frac{\partial\bar{P}}{\partial\theta}\right)d\theta\,d\bar{z}+\int_0^1\int_0^{2\pi}\frac{1}{\bar{h}^3}d\theta\,d\bar{z} \quad \text{... (16)}$$

3.6 Validation of the Developed Model

The model that is developed and presented in the dimensionless form by Eq.8 is compared to the outcomes of existing literature (Pinkus & Sternlicht, 1961) by reducing it to standard Reynolds equation. Table 1 shows the validation of present work with Newtonian fluid (n=1), without any slip condition (B_{1x}=B_{1z}=B_{2x}=B_{2z}=0) with the existing literature.

It is observed that attitude angle, flow rate, and Sommerfeld number are found in good agreement with the available literature.

Table 1: Comparison of current work with the prevailing literature for δ=0.75

L/D	ε	Φ		S	
		*Source	Present	*Source	Present
1	0.4	50	51.84	0.12	0.118
	0.6	50	51.96	0.071	0.069
	0.8	45	46.24	0.039	0.035

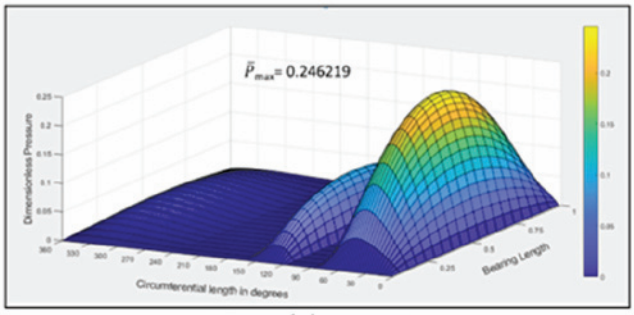
*Source: (Pinkus & Sternlicht, 1961)

3.7 Outcomes and Discussion

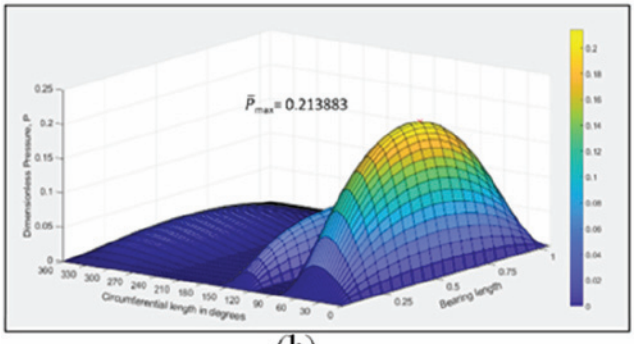
Fig.4(a)-(c) displays the variation in dimensionless pressure for a non-Newtonian lubricant at eccentricity ratios of ε = 0.4, B_{1x}=0.4 and L/D=1 for the three-lobe journal bearing with an ellipticity ratio, δ = 0.5 for varying values of power law index. Fig.4d. displays the dimensionless pressure developed over the circumferential direction of three lobe journal bearing at its mid-plane for varying power-law index values. It is observed that the dimensionless pressure increases with the rise in power-law index values.

The variation of Sommerfeld number for various n values and for δ = 0.75 when B_{1x} = 0.2 and B_{2x} = 0.2 is presented in Fg.5a and 5b respectively. B_{1x} and B_{2x} indicates that the journal surface and bearing surface slip respectively.

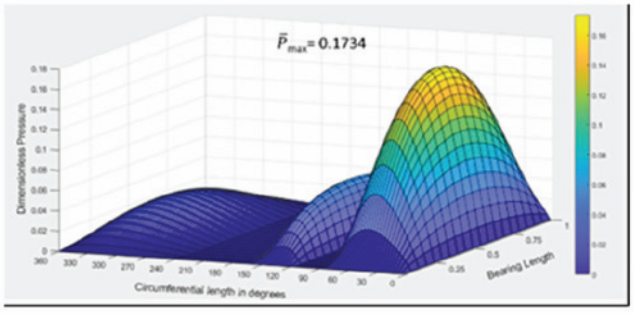
In both circumstances, regardless of the surface, the



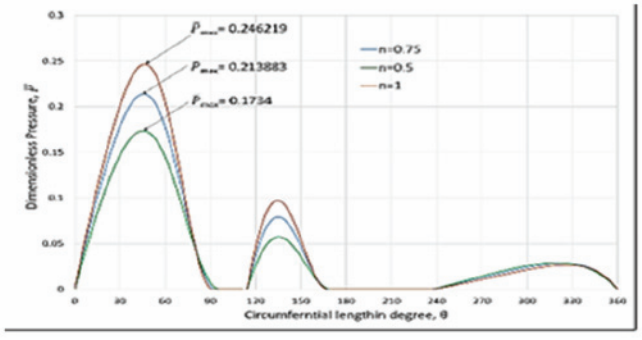
(a)



(b)



(c)



(d)

Figure 4: Variation of dimensionless pressure in a three-lobe bearing at ε=0.4, B_{1x}=0.4, L/D=1 and δ=0.75 varying values of n. (a) n=1, (b) n=0.75, (c) n=0.5, (d) comparison of pressure

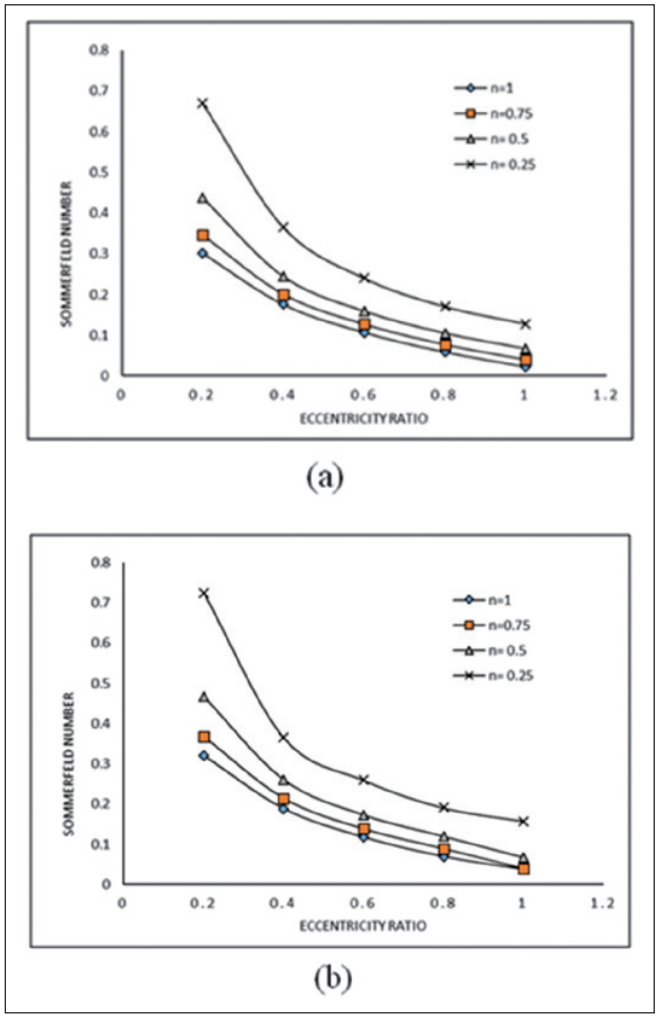


Figure 5: Disparity of Sommerfeld number (a) slip measured on the surface of journal, B_{1x} = 0.2 (b) slip measured on surface of bearing B_{2x} = 0.2

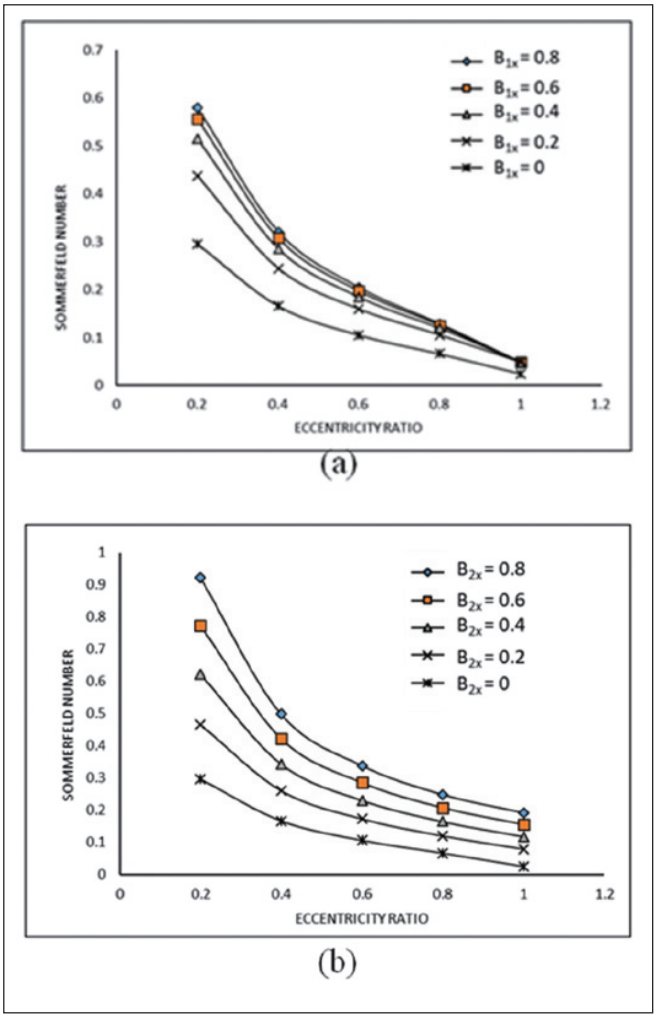


Figure 6: variation of Sommerfeld Number, for $\delta = 0.75$ and $n = 0.5$ for changing values of slip lengths. (a) slip considered on the surface of the journal (b) slip considered on the surface of the bearing

Sommerfeld number drops as the eccentricity ratio increases. Hence, for an assumed length of slip on either the bearing or journal surface, Sommerfeld number will be less for higher eccentricity ratio and a higher value of *n*.

The variation of Sommerfeld number for varying slip-lengths, B_{2x} and B_{1x} for δ=0.75 is presented in Fig.6a and 6b respectively to determine the outcome of wall-slip on a particular surface.

It can be observed that with increase in the magnitude of slip lengths, Sommerfeld number rises for a given eccentricity ratio in both the circumstances of wall-slip. The Sommerfeld number at eccentricity ratio, $\varepsilon = 0.2$ varies roughly from 0.3 to 0.6 when the wall-slip is considered on the surface of journal, whereas, it differs coarsely from 0.3 to 0.95 when-slip is considered on the surface of bearing. This conversely indicates lower pressure development capability in the situation when slip occurs on the wall of the surface of the bearing.

A graph is drawn to estimate the outcome of wall-slip on the load carrying capacity of a journal bearing with three lobes and is illustrated in Figs.7a and 7b.

These graphs represent the variation of dimensionless load for varying slip-lengths, B_{1x} and B_{2x} at δ=0.75, n=0.5 and L/D = 1.0. It can be shown that a smaller slip-length, B_{ix}=0.2, yields a larger load bearing capacity independent of surface type (i=1 or 2). The maximum dimensionless load of 0.45 is achieved by the bearing with slip on journal surface which is approximately 15.38% greater than that achieved by the bearing with wall-slip on the surface of the bearing.

The variation of dimensionless flow rate with eccentricity

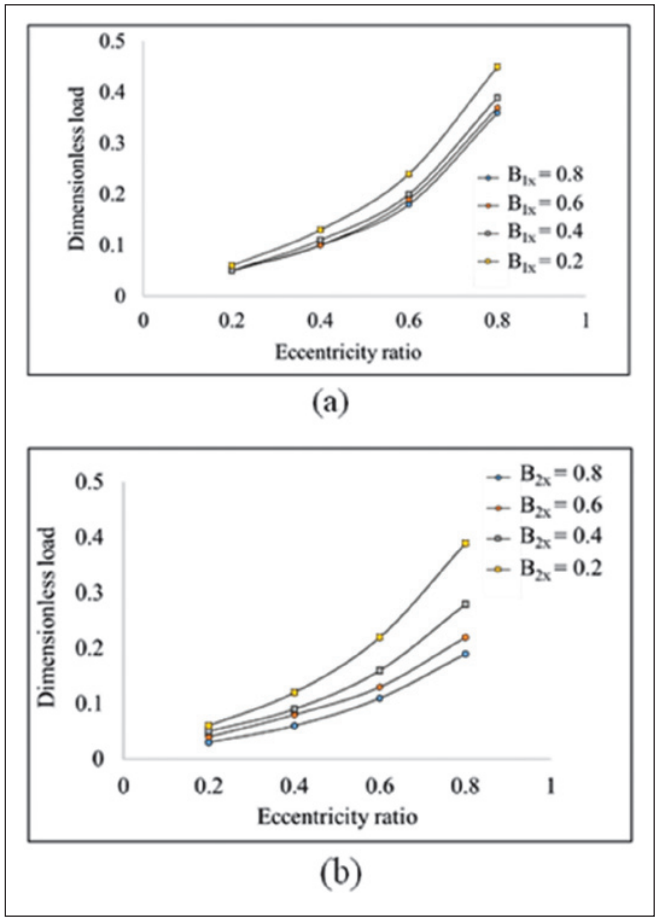


Figure 7: variation of dimensionless load, for $\delta = 0.75$ and n=0.5 for changing values of slip lengths on the surface of journal (a) slip considered on surface of the journal (b) slip considered on the surface of the bearing

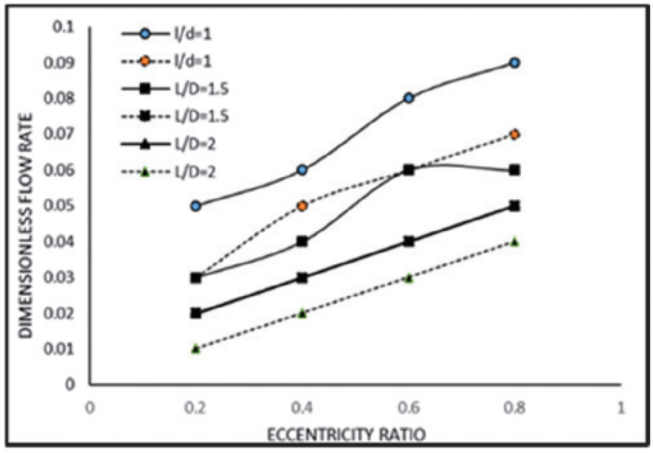


Fig.8: Variation of dimensionless flow rate

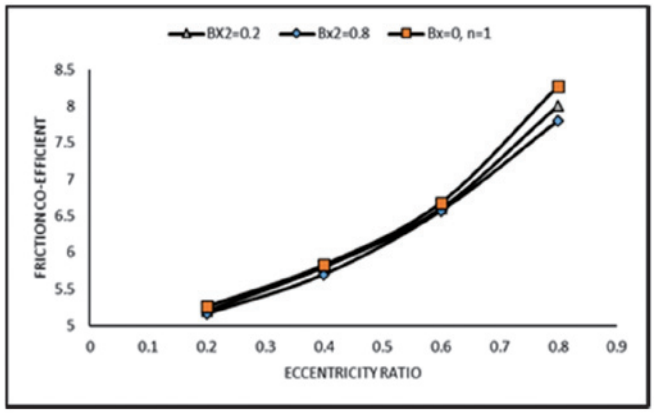


Fig.9: Variation of coefficient of friction

ratio for varying slip lengths and L/D ratio are presented in Fig.8. As eccentricity ratio increase, the volume flow rate is also increased. This is due to the reason that, at higher ratio of eccentricity, the movement of the shaft is higher, thereby leading to high volume flow rate of the lubricant. Also, the flow rate is comparatively high when slip is measured on the surface of journal as compared to slip on the surface of the bearing owing to the fact that, the pressure developed is larger in the former case. The volume flow rate decreases with increase in the L/D ratio.

Fig.9 displays the fluctuation coefficient of friction with eccentricity ratio for various slip lengths and no-slip conditions. It is detected that because of higher shear between the oil layers at higher speeds and the chances of journal touching the bearing surface with surge in eccentricity ratio, the dimensionless friction increases with the rise in eccentricity ratio. Also, when slip is considered on any of the surfaces, the dimensionless friction coefficient is less comparatively as compared to the surface without slip.

4.0 Conclusions

Modified Reynolds equation has been derived for a three-lobe bearing considering slip condition and operating without a Newtonian lubricant. The modified equation is then validated with the available literature by reducing it to no-slip and Newtonian conditions. The following conclusions are drawn after carrying out the static performance analysis.

Higher value for dimensionless pressure is found on a bearing operating with a lubricant having higher value of n=0.5 and lower value of slip length. The dimensionless pressure value was high when the slip was considered on the journal surface. It was discovered that the load carrying capacity was high and exceeded by around 15.38% for the bearing operated with a non-Newtonian lubricant and with slip on the journal surface. The dimensionless friction coefficient was observed to be comparatively less, when the slip occurs on either of the surfaces as compared to the surface without slip.

Nomenclature

b_{ix} - i^{th} surface slip length along x-direction, m, $B_{ix} = \frac{b_{ix}}{C}$, i=1,2

b_{iz} - i^{th} surface slip length along y-direction, m, $B_{iz} = \frac{b_{iz}}{C}$, i=1,2

C - major axis clearance, m

C_m - minor axis clearance, m

d - Radial offset distance of lobe from bearing center, m

D - Journal diameter, m

e - Eccentricity, m

F - Friction force,

$$N\,\bar{F} = \int_0^1 \int_0^{2\pi} \frac{\bar{h}}{2} \frac{\partial \bar{P}}{\partial \theta} d\theta\, d\bar{z} + \int_0^1 \int_0^{2\pi} \frac{1}{\bar{h}} d\theta\, d\bar{z}$$

h - Thickness of fluid film, m

L - Length of journal, m

m - Pseudoplastic viscosity constant, Ns/m^2

P - Pressure, N/m^2, $\bar{P} = \frac{pc^{n+1}}{m\omega^n R^{n+1}}$

Q - Side leakage, $\bar{Q} = -\int_0^{2\pi} \frac{\bar{h}}{6} \frac{\partial \bar{P}}{\partial \bar{z}}\Big|_{\bar{z}=1} d\theta$

R - Journal radius, m

S - Sommerfeld number

u - Velocity in y direction, m/s

u_b - Velocity of journal, m/s

u_{ix} - i^{th} face translational speed in x-direction, m/s

U - Journal velocity, m/s

v - Velocity along y axis, m/s

v_{ix} - i^{th} surface translational speed along x-axis, m/s

V_x - Velocity of slide surface along x-axis, m/s

W - Load carrying capacity, N, $\bar{W} = \frac{WC^{n+1}}{m\omega^n R^{n+2} L}$

Z - Coordinate along the bearing axis, $\bar{z} = \frac{2z}{L}$

z - Bearing axial coordinate, m

δ - Ellipticity ratio, d/C

ε - Major clearance based eccentricity ratio, e/C

ε_k - Minor clearance-based eccentricity ratio of k^{th} (left, right and bottom) lobe, e/C_m

μ - Dynamic viscosity of lubricant, Ns/m^2

θ - Circumferential coordinate of lemon bearing, rad

θ_{c1}, θ_{c2} - start and end of cavitation, rad

ϕ - Bearing attitude angle, rad

ϕ_k - Attitude angle of k^{th} (left, right and bottom) lobe, rad

τ - Time in dimensionless form, $\tau = \omega\tau$

ω - Journal angular velocity, rad/sec.

ψ - Assumed attitude angle

5.0 References

[1] A, A. M. and K, Raghunandana. (2022): Stability Analysis of a Lemon Bearing Operating with Non-Newtonian Lubricant Considering Slip between the Sliding Surfaces, *Engineered Science*, vol. 18, pp. 288-298.

[2] Aurelian, F., Patrick, M. and Mohamed, H. (2011): Wall slip effects in (elasto) hydrodynamic journal bearings, *Tribology International*, vol. 44, pp. 868-877.

[3] Bhushan, B., Wang, Y. and Maali, A. (2009): Boundary slip study on hydrophilic, hydrophobic, and superhydrophobic surfaces with dynamic atomic force microscopy, *Langmuir,* vol. 25, pp. 8117-8121.

[4] Chen, C.Y., Chen, Q.D. and Li, W.L. (2013): Characteristics of journal bearings with anisotropic slip, *Tribology International*, vol. 61, pp. 144-155.

[5] Chetti, B. and Crosby, W. A. (2019): Preload effects on the static characteristics of three-lobe journal bearings lubricated with a couple stress fluid, *Industrial Lubrication and Tribology*, vol.71, pp. 1136-1143.

[6] Crosby, W. A. and Chetti, B. (2009): The static and dynamic characteristics of a two-lobe journal bearing lubricated with couple-stress fluid, *Tribology Transactions*, vol. 52, pp. 262-268.

[7] Das, B. J. and Roy, L. (2018): Analysis and comparison of steady-state performance characteristics of two-axial groove and multilobe hydrodynamic bearings lubricated with non-Newtonian fluids, Proceedings of the Institution of Mechanical Engineers, Part J: *Journal of Engineering Tribology*, vol. 232, pp. 1581-1596.

[8]. Fortier, A. E. and Salant, R. F. (2005): Numerical analysis of a journal bearing with a heterogeneous slip/no-slip surface, *Journal of Tribology*, vol. 127, pp. 820-825.

[9]. Khonsari, M. M. and Brewe, D. E. (2008): On the Performance of Finite Journal Bearings Lubricated with Micropolar Fluids, *Tribology Transactions*, vol. 32, pp. 155-160.

[10] Lin, Q., Wei, Z., Wang, N. and Chen, W. (2015): Effect of large-area texture/slip surface on journal bearing considering cavitation, *Industrial Lubrication and Tribology*, vol. 67, pp. 216-226.

[11] Nessil, A., Larbi, S., Belhaneche, H. and Malki, M. (2013): Journal bearings lubrication aspect analysis using non-newtonian fluids. *Advances in Tribology*, vol. 2013, pp. 1-9.

[12] Pinkus, O. and Sternlicht, B. (1961): Theory of hydrodynamic lubrication, McGra-Hill Book Company. Inc, New York.

[13] Rahmatabadi, A. D., Nekoeimehr, M. and Rashidi, R. (2010): Micropolar lubricant effects on the performance of noncircular lobed bearings, *Tribology International,* vol. 43, pp. 404-413.

[14] Rao, T. V. V. L. N. (2010): Analysis of single-grooved slider and journal bearing with partial slip surface, *Journal of Tribology*, vol.132, pp. 1-7.

[15] Rao, T. V. V. L. N., A Rani, A. M., Mohamed, N. M., Ya, H. H., Awang, M. and M Hashim, F. (2019): Static and stability analysis of partial slip texture multi-lobe journal bearings, Proceedings of the Institution of Mechanical Engineers, Part J: *Journal of Engineering Tribology,* vol. 234, pp. 567-587.

[16] Rothstein, J. P. (2009): Slip on Superhydrophobic Surfaces, *Annual review of fluid mechanics*, vol.42, pp. 89-109.

[17] Soni, S. and DP, V. (2015): Static analysis of finite hydrodynamic journal bearing in turbulent regime with non-Newtonian lubricant, *Tribology Online*, vol.10, pp. 246-261.

[18] Spikes, H. A. (2003): The half-wetted bearing. Part 1: Extended Reynolds equation. Proceedings of the Institution of Mechanical Engineers, Part J: *Journal of Engineering Tribology*, vol. 217, pp. 1-14.

[19] Spikes, H. and Granick, S. (2003): Equation for Slip of Simple Liquids at Smooth Solid Surfaces, *Langmuir*, vol. 19, pp. 5065-5071.

[20] Tayal, S. P., Sinhasan, R. and Singh, D. V. (1982): Finite element analysis of elliptical bearings lubricated by a non-Newtonian fluid, *Wear*, vol. 80, 71-81.

[21] Tsai-Wang Huang, Cheng-I Weng and Chao-Kuang Chen. (1988): Analysis of finite width journal bearings with micropolar fluids. *Wear*, vol. 123, pp. 1-12.

[22] Wu, C. (2008): Performance of hydrodynamic lubrication journal bearing with a slippage surface, *Industrial Lubrication and Tribology*, vol.60, pp.293-298.